Supplementary Information

Metal-organic framework derived bimetal oxides $CuCoO_2$ as efficient electrocatalysts for oxygen evolution reaction

Han Gao,[a,b] Miao Yang,[a] Zijuan Du,[a] Xing Liu,[a] Xianglong Dai,[a] Kun Lin,[a] Xiao-Qing Bao,[c] Hong Li,[a] and Dehua Xiong*,[a,b]

a. State Key Laboratory of Silicate Materials for Architectures, Wuhan University of Technology, Wuhan 430070, P. R. China.
b. Wuhan National Laboratory for Optoelectronics, Huazhong University of Science and Technology, Wuhan 430074, P. R. China.
c. State Key Laboratory of Optical Technologies on Nanofabrication and Microengineering, Institute of Optics and Electronics, Chinese Academy of Sciences, Chengdu 610209, P. R. China.

* Corresponding author email: xiongdehua2010@gmail.com

Experimental details

Materials synthesis

The chemicals in these experiments were analytical grade products purchased from Sigma Aldrich without further processing. The metal-organic frameworks (MOF) derived $CuCoO_2$ (CCO) nanocrystals were synthesized by a solvothermal method, following our previous work (*Inorg. Chem. Front.* 2018, 5, 183-188., *New J. Chem.* 2019, 43, 15233-15239.) Typically, Cu-BTC (Cu-BTC samples were purchased from Nanjing XFNANO Materials Tech Co., Ltd.) and ZIF-67 (ZIF-67 powders were prepared by the previous method) were dissolved in the deionized water (DI) and anhydrous ethanol (ET) mixture. Then a certain amount of NaOH was added to the solution, and the mixture was stirred for 30 minutes. Finally, the above solution was put into a high-pressure reactor and reacted at different temperatures for 24 hours. After the reaction, the obtained powders were washed with absolute alcohol and deionized water several times.

Structural characterizations

The crystal phase of samples was characterized by the powder X-ray diffraction (XRD, D8 Advance). The microstructure, morphology, and composition of as-synthesized MOF-CCO samples were observed using the transmission electron microscopy (TEM, FEI Titan ChemiSTEM operating at 200 keV) coupled with energy-dispersive X-ray spectroscopy (EDX) and the field-emission scanning electron microscopy (FESEM, QUANTA FEG 450) coupled with EDX. The surface chemical states of MOF-CCO powders were analyzed by X-ray photoelectron spectroscopy (XPS, Thermo Escalab 250Xi). And the C 1s line (284.80 eV) corresponding to the surface adventitious carbon (C-C line bond) has been used as the reference binding energy. The Brunauer-Emmett-Teller (BET) specific surface areas and porosity parameters of the samples were taken by the N_2 adsorption-desorption isothermetry (Micromeritics TriStar II 3020 3.02). The particle size distribution and average particle size of the sample were determined by Zeta ZS90 & Mastersizer 3000.

Electrode preparation and electrochemical measurement

Firstly, 15.0 mg MOF-CCO or CCO powder was added into 500 μL deionized water, 480 μL isopropanol and 20 μL Nafion mixture, and the suspension containing MOF-CCO powder was obtained by ultrasonic dispersion. The 20.00 μL suspension was dripped on the nickel foam with a working area of 1 x 1 cm^2. And then the electrode was dried (at 150 °C for 5 min) for the electrochemical measurements. The MOF-CCO loading mass of these electrodes was kept at 0.30 mg cm^{-2}.

The OER performance was evaluated by the cyclic voltammetry (CV) and electrochemical impedance spectroscopy (EIS) in a three-electrode configuration in 1.0 M KOH (pH = 13.5) using a CS2350H electrochemical workstation (Wuhan Corrtest Instruments Corp., China). A platinum wire and a saturated calomel electrode (SCE) were used as the counter electrode and reference electrode, respectively. The CV scans were recorded between 1.05 and 1.80 V vs. reversible hydrogen electrode (RHE) at the scan rate of 5 mV s^{-1}. The electrochemical double-layer capacitance (C_{dl}) of each sample was measured given that C_{dl} is positively proportional to the effective surface areas (ESA). C_{dl} can be extracted through CV scans at different rates (from 20 to 100 mV s^{-1}) in the non-faradaic potential window of -0.05 to 0.05 V vs. SCE. The EIS measurements were performed in the frequency range of 20 mHz - 200 kHz under a constant potential of 1.60 V vs. RHE.

All current density values were normalized with respect to the geometrical surface area of the working electrode. All CV curves presented in this work were iR-corrected. The correction was done according to the following equation:

$$E_c = E_m - iR_s, \quad (1)$$

where E_c is the iR-corrected potential, E_m is the experimentally measured potential, and R_s is the equivalent series resistance extracted from the Zero-Input Response (ZIR) measurements. Unless otherwise specified, all potentials were reported versus the RHE by converting the potentials measured vs. SCE according to the following formula:

$$E\ (RHE) = E\ (SCE) + 0.241 + 0.059\ pH \quad (2)$$

Supplementary Tables:

Table S1. Detailed reaction conditions employed to synthesize MOF-derived delafossite $CuCoO_2$ nanocrystals.

<table>
<tr><th>No.</th><th>ZIF-67</th><th>Cu-BTC</th><th>NaOH /g</th><th>Solvent (ET:DI)/mL</th><th>Temperature /°C</th><th>Time /h</th><th>Theoretical yield/mg</th></tr>
<tr><td>1</td><td rowspan="12">0.10g/ 0.45mmol</td><td rowspan="5">0.10g/ 0.17mmol</td><td rowspan="8">2.00</td><td>0:70</td><td rowspan="3">140</td><td rowspan="14">24</td><td rowspan="12">69.52</td></tr>
<tr><td>2</td><td>35:35</td></tr>
<tr><td>3</td><td rowspan="11">50:20</td></tr>
<tr><td>4</td><td>120</td></tr>
<tr><td>5</td><td>100</td></tr>
<tr><td>6</td><td>0.12g/ 0.20mmol</td><td rowspan="9">140</td></tr>
<tr><td>7</td><td>0.14g/ 0.23mmol</td></tr>
<tr><td>8</td><td>0.16g/ 0.26mmol</td></tr>
<tr><td>9</td><td rowspan="4">0.10g/ 0.17mmol</td><td>4.00</td></tr>
<tr><td>10</td><td>5.00</td></tr>
<tr><td>11</td><td>6.00</td></tr>
<tr><td>12</td><td>7.00</td></tr>
<tr><td>13</td><td>0.50g/ 2.24mmol</td><td>0.50g/ 0.83mmol</td><td rowspan="2">5.00</td><td>346.03</td></tr>
<tr><td>14</td><td>1.00g/ 4.48mmol</td><td>1.00g/ 1.65mmol</td><td>692.07</td></tr>
</table>

Table S2. The OER activity of Ni@MOF-CCO1 electrode in comparison to that of other delafossite oxides as well as other ternary metal oxides OER catalysts recently reported in the literatures.

Catalyst	Electrolyte	η value at 10 mA cm^{-2} (mV)	Tafel plot (mV dec^{-1})	Ref (year)
Bare Ni	1.0 M KOH	473.2	117.8	This work
Ni@CCO		407.5	90.2	
Ni@MOF-CCO1		364.7	64.1	
Ni@MOF-CCO2		387.3	86.1	
glassy carbon@CCO		440.0	92.8	[27] (2018)
glassy carbon@CCO-PVP		390.0	70.0	[28] (2019)
Ni@CCCO-PVP		470.0	96.5	[26] (2020)
Ni@$CuScO_2$		470.0	114.0	[18] (2020)
glassy carbon@$AgCoO_2$		395.0	-	[52] (2019)
glassy carbon@$NdBaMn_2O_{5.5}$		-	75.0	[53] (2018)
glassy carbon@$La_{1-x}Sr_xCoO_{3-\delta}$		326.0	70.8	[54] (2018)
glassy carbon@ $Sr_2Fe_{1.5-x-y}Co_xNi_yMo_{0.5}O_{6-\delta}$	0.1 M KOH	400	84	[55] (2019)
glassy carbon@$LaNiO_3$		550	148	[56] (2019)
glassy carbon@$LaNi_{0.85}Mg_{0.15}O_3$		450	95	[56] (2019)
glassy carbon@$LaCoO_3$		680 vs Ag/AgCl	74.4	[57] (2019)
glassy carbon@$LaCo_{0.9}Ni_{0.1}O_3$		650 vs Ag/AgCl	64.2	[57] (2019)
glassy carbon@$LaCo_{0.7}Ni_{0.3}O_3$		657 vs Ag/AgCl	72.8	[57] (2019)
glassy carbon@$LaCo_{0.5}Ni_{0.5}O_3$		660 vs Ag/AgCl	73.9	[57] (2019)

Supplementary Figures:

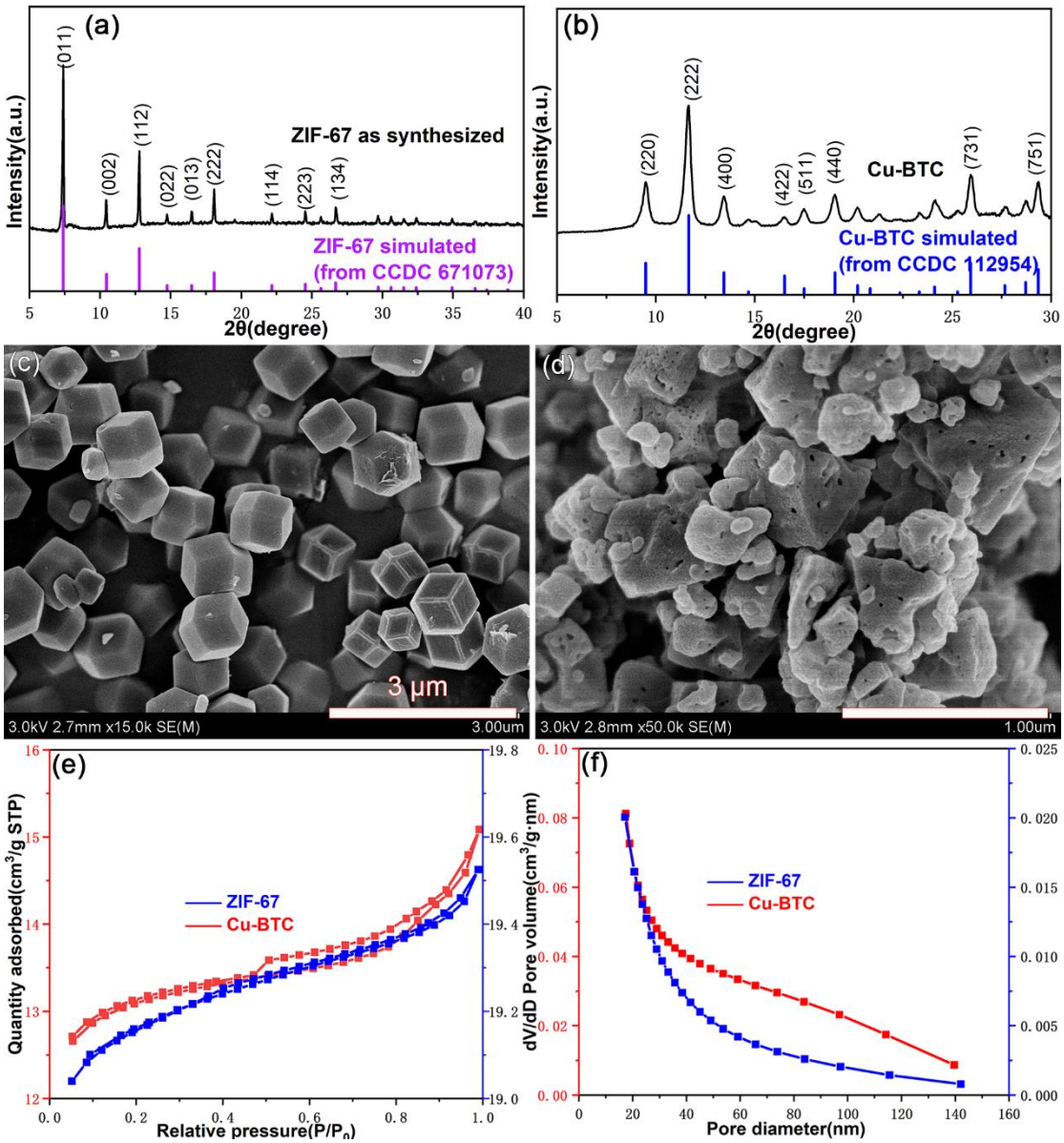

Fig. S1. XRD patterns ((a) ZIF-67, (b) Cu-BTC), SEM images ((c) ZIF-67, (d) Cu-BTC), Nitrogen adsorption-desorption isotherm plots (e), and BJH pore-size distribution curves (f) of ZIF-67 and Cu-BTC powders.

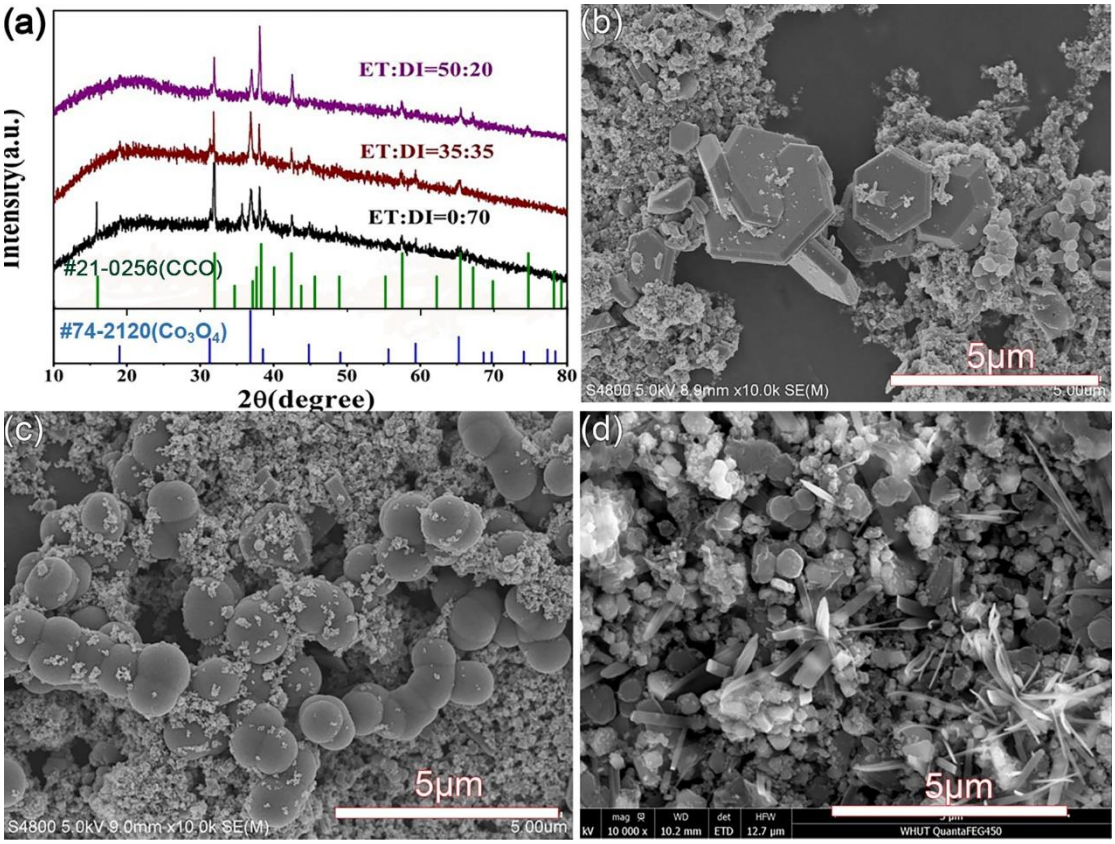

Fig. S2. XRD pattern (a) and SEM images ((b) ET:DI=0:70, (c) ET:DI=35:35, (d) ET:DI=50:20) of the products with different proportions of anhydrous ethanol and deionized water.

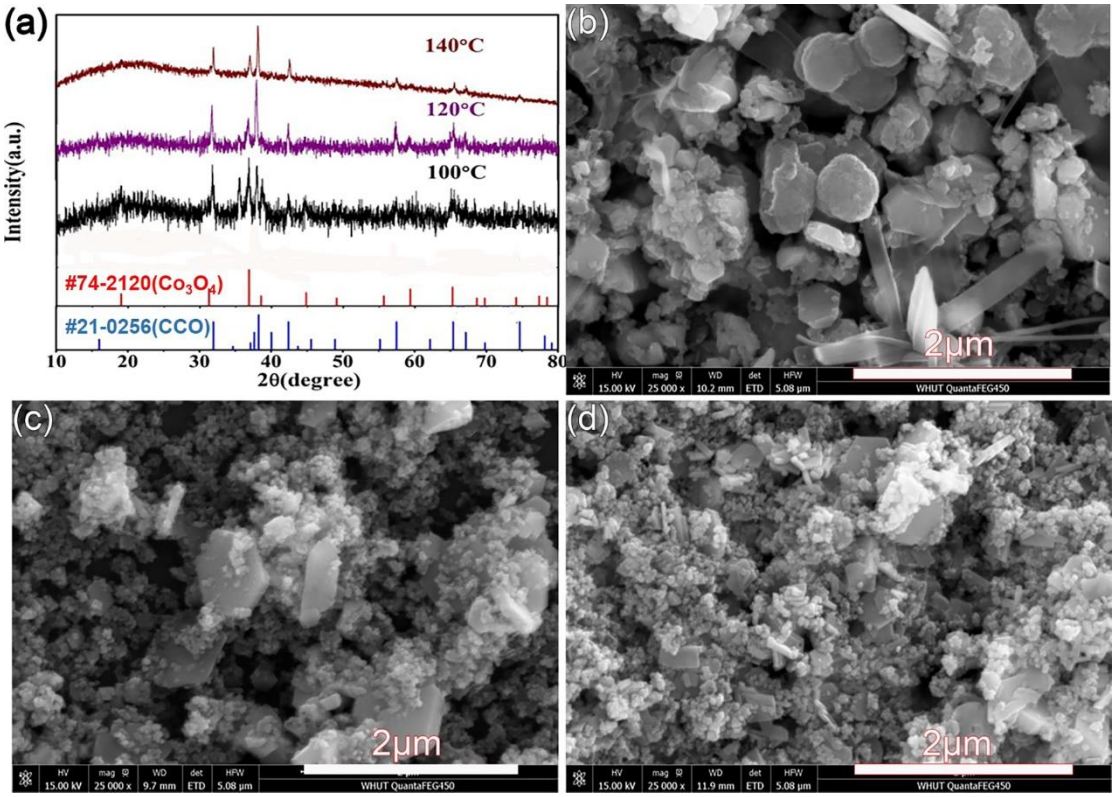

Fig. S3. XRD pattern (a) and SEM images ((b) 140 ℃, (c) 120 ℃, (d) 100 ℃) of products with different temperatures.

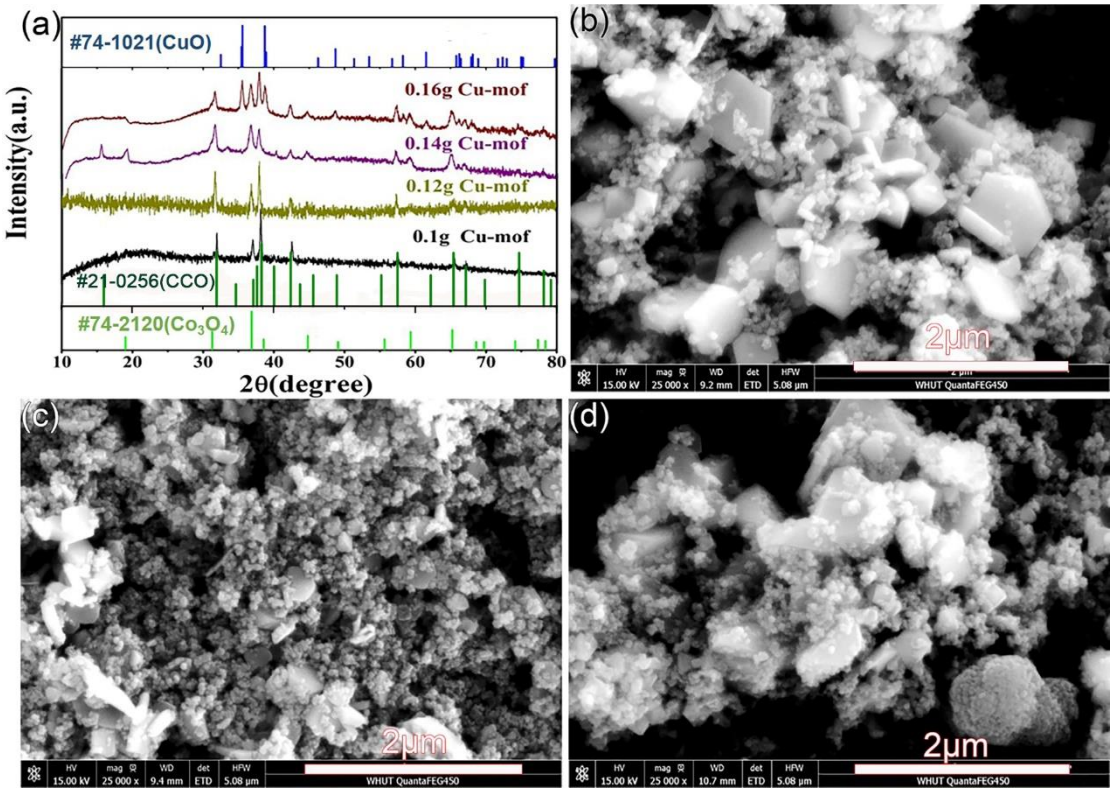

Fig. S4. XRD pattern (a) and SEM images ((b) Cu-BTC/ZIF-67 = 1.2 :1, (c) 1.4:1, and (d) 1.6:1) of the products obtained by solvothermal synthesis with different mass ratio of reactants.

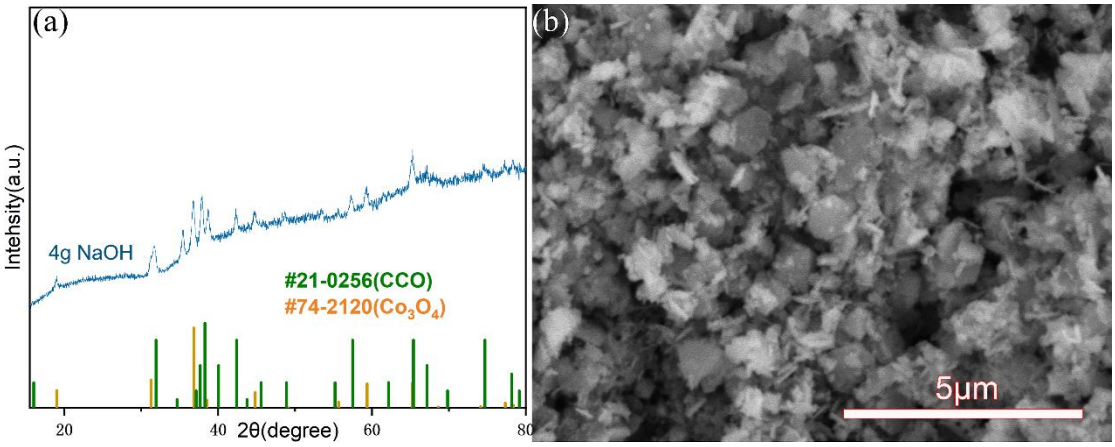

Fig. S5. XRD pattern (a) and SEM image (b) of the product obtained by the solvothermal synthesis with 4.00 g NaOH addition.

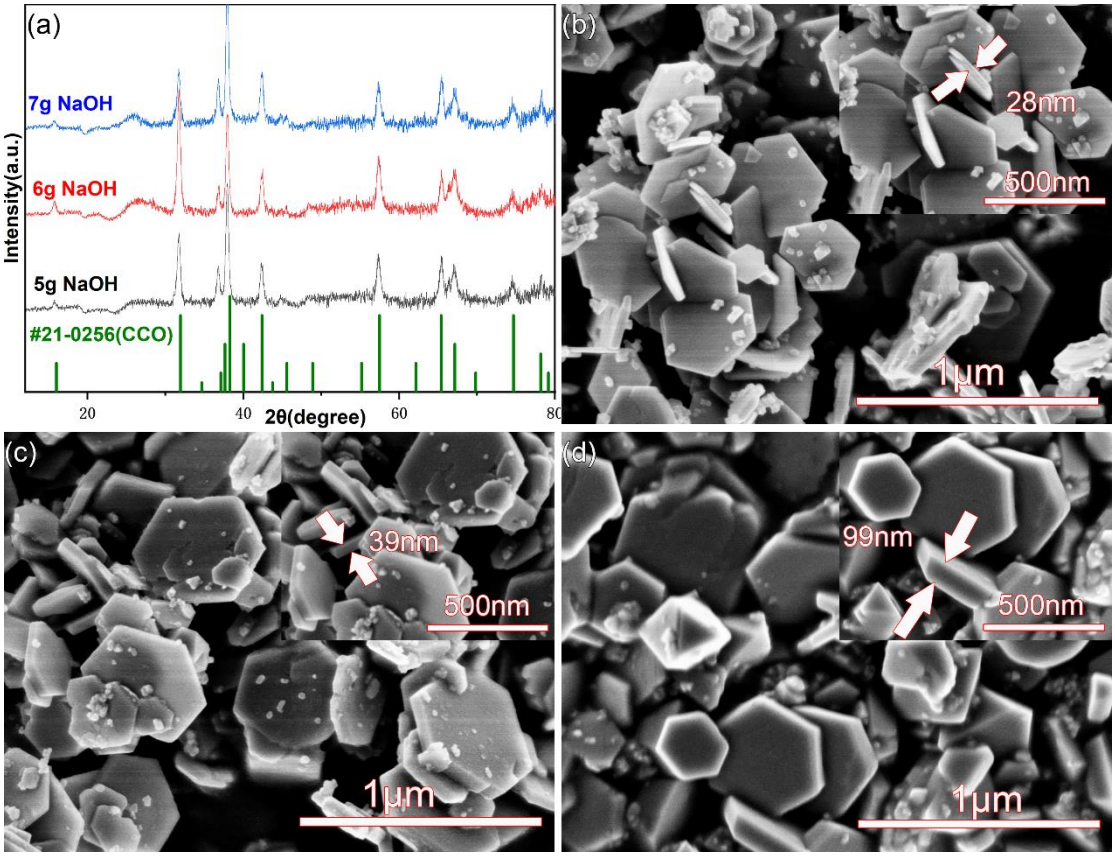

Fig. S6. XRD pattern (a) and SEM images ((b) 5.00 g, (c) 6.00 g, (d) 7.00 g NaOH) of the product obtained by the solvothermal synthesis with different NaOH addition.

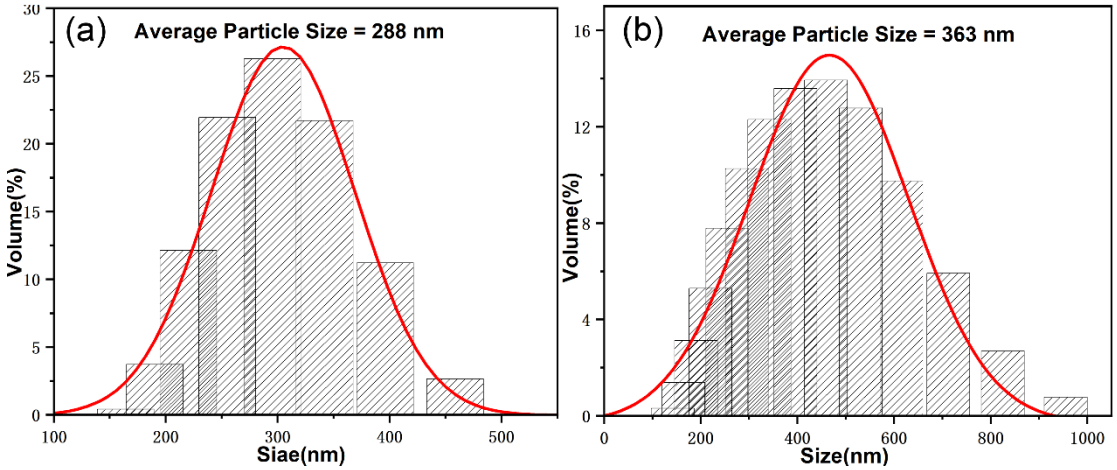

Fig. S7. The partical size distributions of MOF-CCO1 (a) and MOF-CCO2 (b).

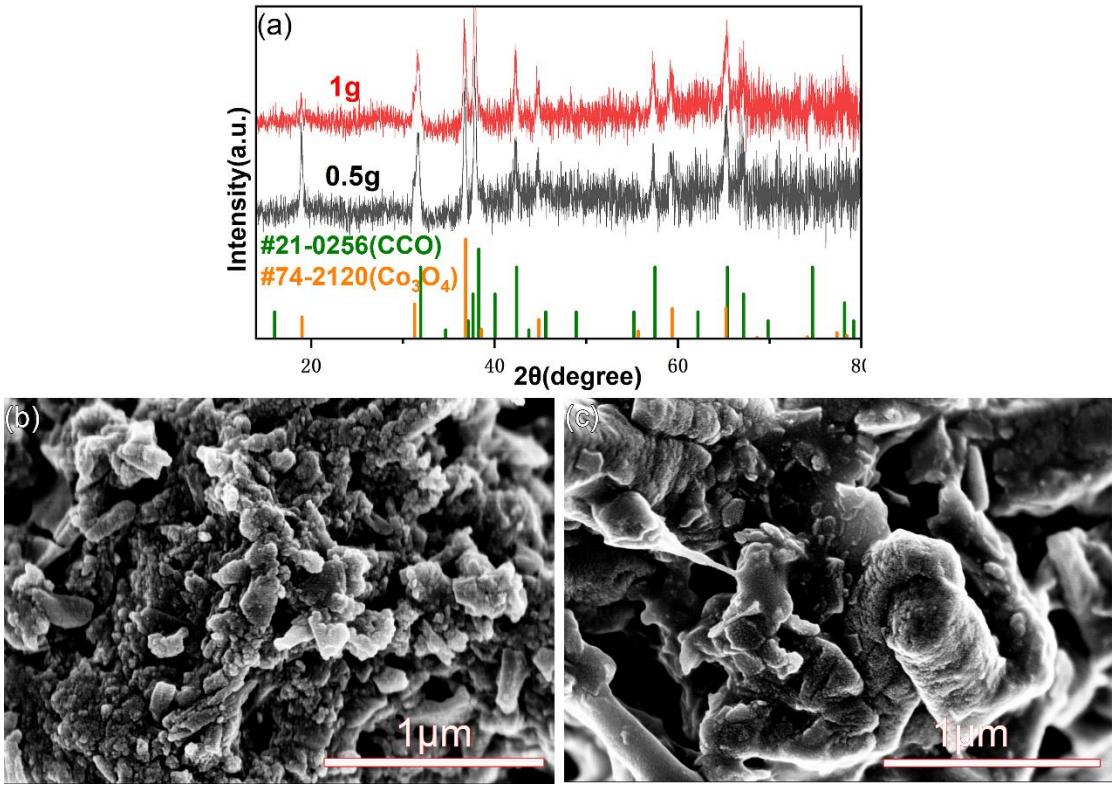

Fig. S8. XRD pattern (a) and SEM images of the products obtained by the solvothermal method when the amount of reactants all increased by 5 (b) and 10 (c) times.

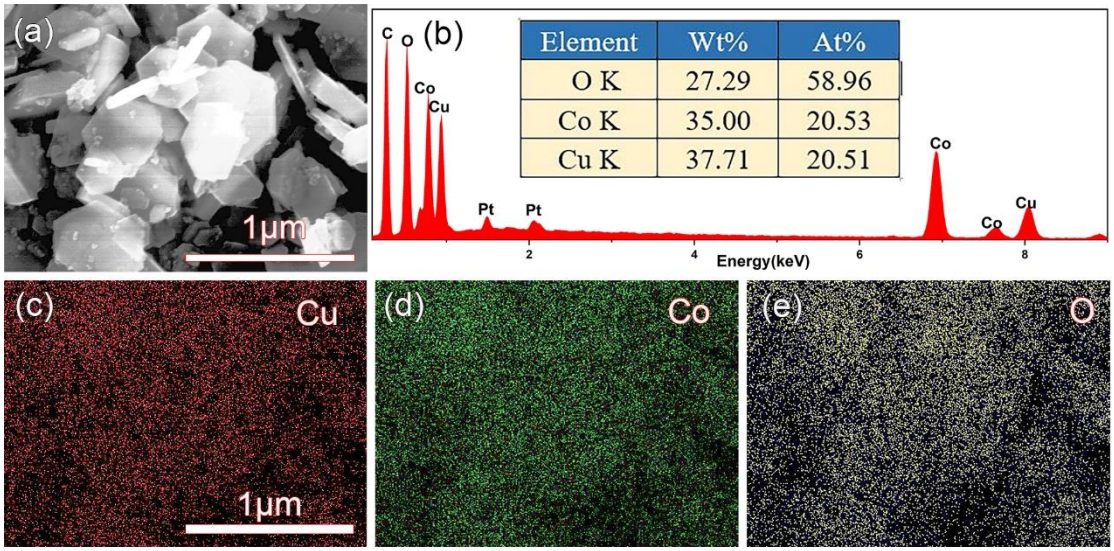

Element	Wt%	At%
O K	27.29	58.96
Co K	35.00	20.53
Cu K	37.71	20.51

Fig. S9. SEM image (a), elemental analysis report (b), and EDS elemental mappings (c-e) of CCO synthesized by the solvothermal method with 5.00 g NaOH addition.

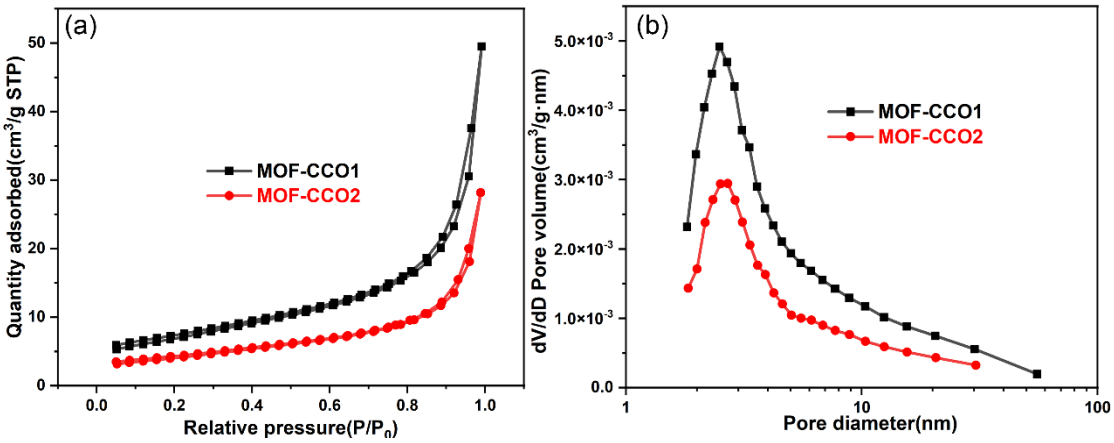

Fig. S10. Nitrogen adsorption-desorption isotherm plots (a) and BJH pore-size distribution curves (b) of MOF-CCO1 and MOF-CCO2 powders.

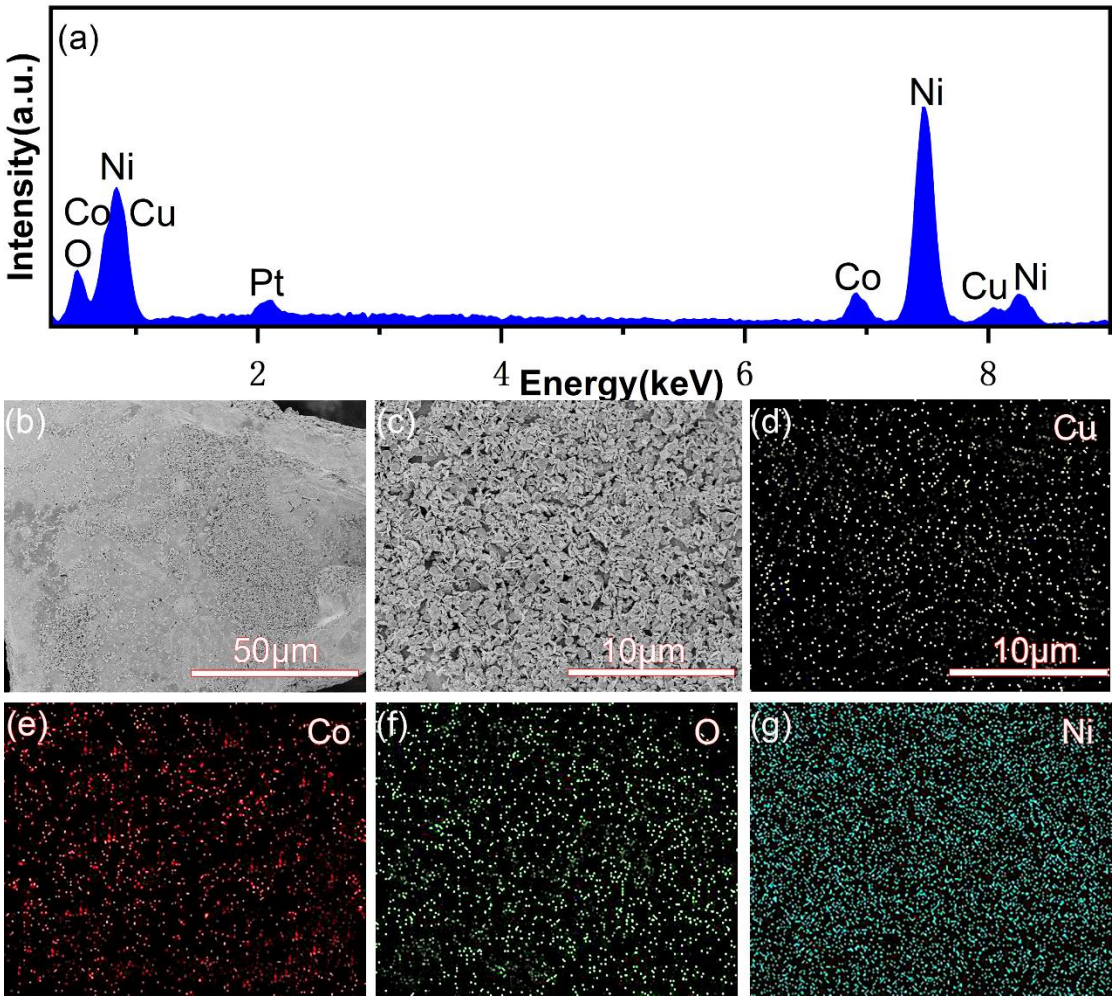

Fig. S11. EDX spectrum (a), SEM image (b), and elemental maps (c-g) of Ni@MOF-CCO1 before OER measurement.

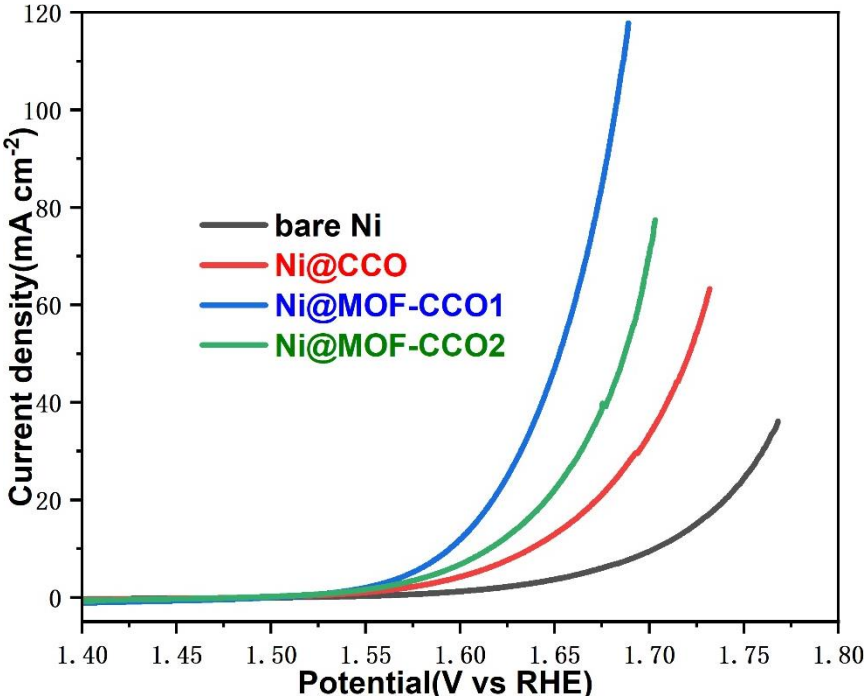

Fig. S12 The reduction branch of the CV curves (Fig. 3a) of bare Ni, Ni@CCO, Ni@MOF-CCO1, and Ni@MOF-CCO2 working electrodes.

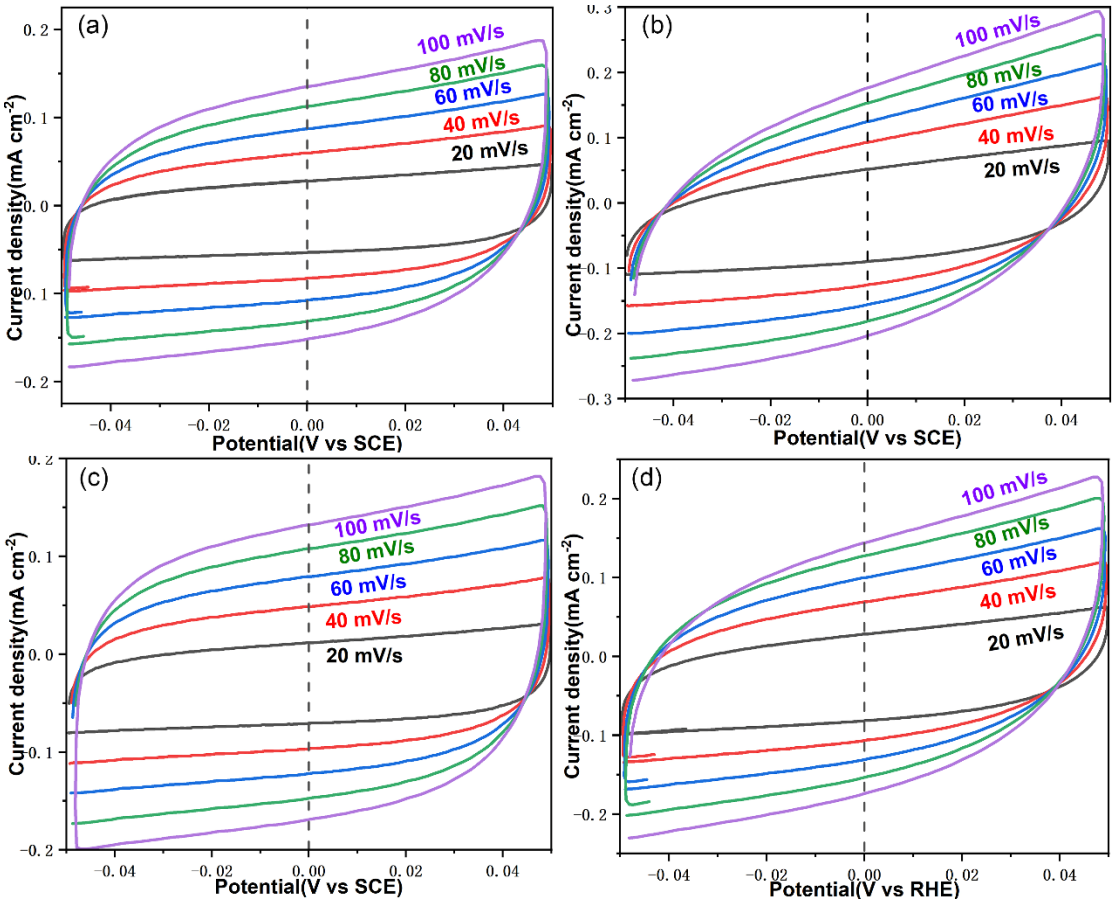

Fig. S13. CV curves of bare Ni (a), Ni@CCO (b), Ni@MOF-CCO1 (c), and Ni@MOF-CCO2 (d) working electrode measured in 1.0 M KOH in the non-Faradaic region with different scan rates from 20 to 100 mV s^{-1}.

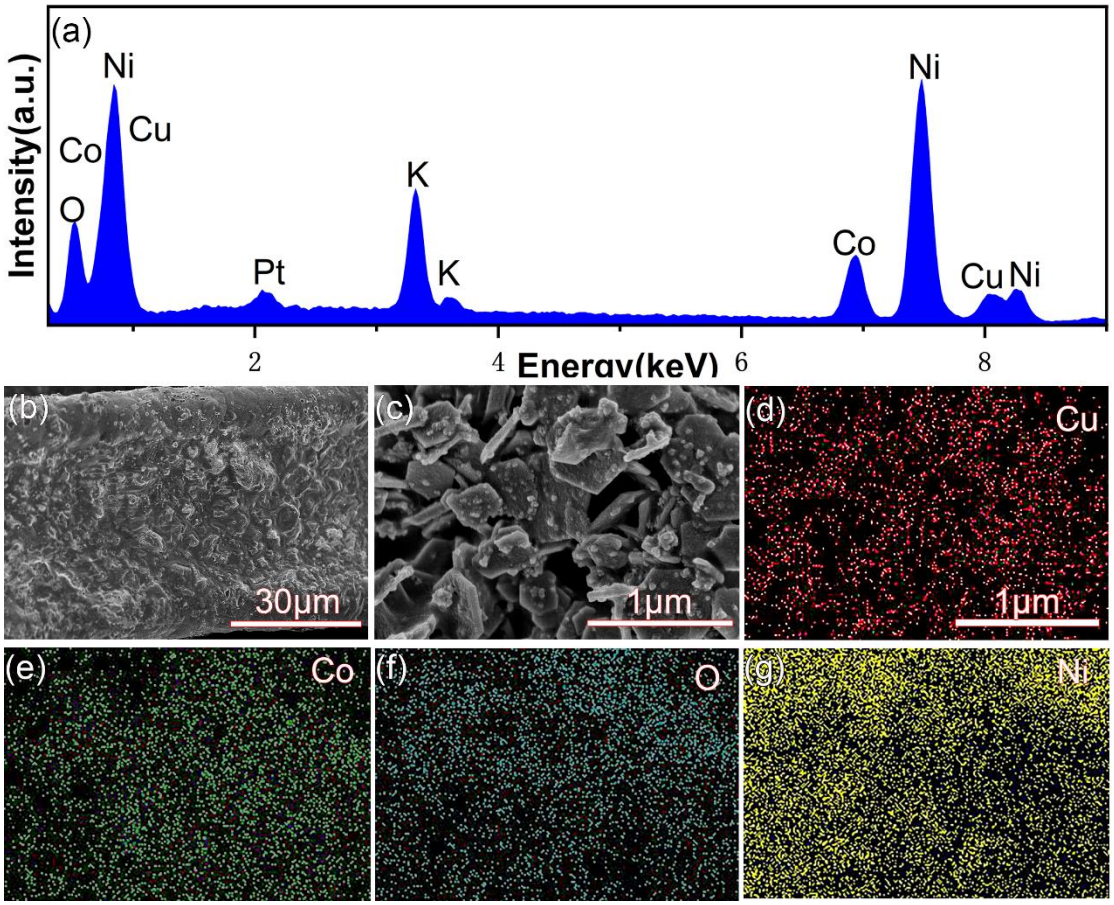

Fig. S14. EDX spectrum (a), SEM image (b), and elemental maps (c-g) of Ni@MOF-CCO1 after long-term OER measurement.